Identification of ESS Degradations Related to their Uses in Micro-Grids: application to a building lighting network with VRLA batteries

Margot Gaetani-Liseo, Corinne Alonso, Bruno Jammes

The original publication is available at
https://www.iieta.org/journals/ejee/paper/10.18280/ejee.230605
and also at http://www.iieta.org

Identification of ESS Degradations Related to their Uses in Micro-Grids: application to a building lighting network with VRLA batteries

Gaetani-Liseo Margot [1,2*], Alonso Corinne [1,2], Jammes Bruno[1,2]

[1] LAAS-CNRS, 7 avenue du Colonel Roche, BP 54200 31031 Toulouse cedex 4, France
[2] Université Toulouse III - Paul Sabatier, 118 route de Narbonne, 31062 Toulouse cedex 9, France

Corresponding Author Email: mgaetani@laas.fr

https://doi.org/10.18280/ejee.xxxxxx

Received:
Accepted:

Keywords:
battery ageing mechanisms, cycle lifetime, charge protocol, energy storage, Lead-acid battery, micro-grid, PV, VRLA batteries

ABSTRACT

This paper presents a study about power profiles of microgrids with highly intermittent sources and their impacts on energy storage system. We propose an original method to consider the storage system lifetime in the microgrid design process. We present some criteria to quantify the batteries stresses generated by microgrids working operations. The first step of this work is to calculate the power exchanged with the storage system. Thus, we explain a new optimal sizing algorithm using a power/energy model based on datasheets parameters. In a second step, we focus our analysis on the potential damages on valves regulated lead acid batteries because it is the most used storage system in case of stationary applications for urban microgrids. The damages reviewed allow us to put forward five indexes calculated thanks to the power profiles. With this point of view, we optimize the batteries uses without lifetime model in both contexts: microgrid design and energy management. We observe the evolution of these indexes to different size configurations determined with our sizing method applied to the photovoltaic production and the lighting network consumption of the building laboratory. We choose to compare four configurations that all ensure autonomy: two determined with Pareto optimization method and two critical cases corresponding to the minimal and the maximal values of the size of the energy storage system into the entire possible configuration tested.

1. INTRODUCTION

The climate change, the fossil resources depletion and the recent environmental considerations for the planet preservation motivate scientists to found a cleaner and more efficient way to produce and distribute the electrical energy. With this challenge, research interests in microgrids (MG) dedicated to supply building have gained a wide international attention during the last few years [1] [2] [3]. These new MG integrate distributed electrical sources, such as renewable energy sources (RES), associated with energy storage systems (ESS). They can be connected to the main distribution grid or operate in isolated mode. To be competitive they have to be efficient, functional and sustainable [4]. The main technical difficulties to design these MG is to deal with RES intermittencies, which depend on climate conditions, while we optimize the use of the ESS in term of economical and environment costs.

In this context, enhance the ESS lifetime represents a high technical challenge [5]. This lifetime depends on the energy flow during operations and so on the energy/power management systems (EMS/PMS) [6] [7] and on the ESS sizing (quantity of energy, capacity, power range, topology and technological choices), which are themselves related [8] [9]. Thus, to define the optimal MG configuration it is important to take into account the ESS stress mechanisms involving potentials degradations and prematurely ESS lifetime decrease. In the state of the art, numerous methodologies propose to find the optimal ESS sizing and their EMS associated [8]. These methods integrate the ageing estimation thanks to lifetime models often complex and resulting of long and specific ageing experiments [5]. Furthermore, these models depend on the ESS technologies and it appears premature to consider such detailed model. In fact, the optimization criteria become difficult to define and to integrate in the design optimization process. Our proposal is to focus on the ESS degradations and then to establish links between power exchanges and ESS damages. Authors in [10] and [11] proposed to analyze the ESS operating conditions, as the current variations, in order to identify operations that provoked premature failure on ESS. Analysis presented in [11] proposes a classification of different existing MG according to their uses until the ESS achieve their end of life. The authors correlate the ESS damages with the power profile variations and thus propose some indicators to qualify the MG. The advantage of this analysis is that the indicators reflects one or few degradations and are independent of any kind of ageing model. We can assume that optimizing these indexes during the MG design ensure a longer ESS lifetime. Thereby, our approach consists in estimating a set of indicators deduced from the power profiles fluctuations. This approach is independent of any specific model of ESS, only based on

information issued from technical datasheets. With this method, we optimize the uses and we do not need ageing model. This algorithm permits to generate the power profile and help to size the ESS and the RES. We define a set of relevant criteria quantifying the benefits and the drawbacks of ESS uses according to the degradations reviewed in the literature. Finally, we calculate these criteria on the power profiles generated for different sizes of ESS and RES in order to qualify the operating conditions and the sizing. We apply this methodology in the case of a self-sufficient application and the criteria proposed in this paper correspond to the stress mechanisms of valve regulated lead acid batteries (VRLAB) or sealed lead acid batteries. One of the advantages of our sizing algorithm consists on using only datasheet to generate the power profiles thus allowing an easy comparison of several types of ESS technologies.

In the following section, we present the algorithm enabling the optimal ESS design. In section 3, we review the main VRLAB behaviors and the potential damages able to occur in order to give the optimal working conditions that improve the battery lifetime. In section 4, we detail the results of our sizing methodology applied to the lighting network of the laboratory building integrated photovoltaics (BiPV). Then, to validate our approach we compare four different configurations according to criteria given in section 3. Finally, in section 5, we give some perspectives of this work.

2. POWER PROFILES AND ESS SIZE

2.1 General sizing methodology

Figure 1 presents the flowchart of the proposed algorithm able to size the ESS and the production sources, in our case photovoltaic generators (PV), as explain in the next subsection. First, we define $P_{BAL}(t)$ with equation (1) as the difference between the production power, $P_{PROD}(t)$, and the consumption power, $P_{LOAD}(t)$, considered positive and negative respectively. Then, we calculate the $E_{BAL}(t)$ energy profile by integrating $P_{BAL}(t)$ as described by equation (2).

$$P_{BAL}(t) = P_{PROD}(t) + P_{LOAD}(t) \quad (1)$$

$$E_{BAL}(t) = E_{BAL}(t - \Delta t) + P_{BAL}(t - \Delta t) * \Delta t \quad (2)$$

We verify that $E_{BAL}(t)$ at t_{LIM} is superior or at least equal to the energy at the beginning t_0, of the time horizon T. This condition ensures that production is sufficient to charge the ESS until time t_{LIM}. If $E_{BAL}(t_{LIM})$ is inferior to $E_{BAL}(t_0)$ we have to increase the size of the PV plants or/and authorizing the access to the main grid. If $E_{BAL}(t_{LIM})$ is higher than $E_{BAL}(t_0)$, we determine the largest decrease on the energy profile $E_{BAL}(t)$ in the time horizon T, called ΔE. ΔE represents the minimum ESS size to ensure the autonomy, considering the ESS with a 100% efficiency with no losses and no limit on power rate. At the first iteration in the algorithm, ΔE_{ESS} is set to the value of the calculated ΔE. After this step, the validation block allows to calculate the power profile exchanged with the ESS, noted $P_{ESS}(t)$. These values highly depends on the ESS model and the power limitations introduced in the algorithm and corresponds to the part of the $P_{BAL}(t)$ profile exchanged through the ESS having the size ΔE_{ESS}. Thanks to the systems of equations (3) and (4) described below, we determine in cases of charge and discharge the variables $P_{ESS}(t)$, $P_{DEF}(t)$ and $P_{EX}(t)$, with $P_{DEF}(t)$ the deficit power and $P_{EX}(t)$ the power in excess. In these equations, the power limitations in charge and discharge are constant. These parameters $Crate_{MAXc}$ and $Crate_{MAXd}$ are maxima C-rates respectively in charge and in discharge and can be easily obtained from the datasheet. With $P_{ESS}(t)$ we deduce a new $E_{ESS}(t)$ with the equation (5) in charging mode and (6) in discharging mode. In equation (5), η_E is the ESS energy efficiency given in the datasheet.

$$charge \begin{cases} P_{DEF}(t) = 0; \\ if P_{BAL}(t) \leq Crate_{MAXc} * \Delta E_{ESS} \\ P_{ESS}(t) = P_{BAL}(t), P_{EX}(t) = 0; \\ else \begin{cases} P_{ESS}(t) = Crate_{MAXc} * \Delta E_{ESS} \\ P_{EX}(t) = P_{BAL}(t) - P_{ESS}(t) \end{cases} \end{cases} \quad (3)$$

$$discharge \begin{cases} P_{EX}(t) = 0; \\ if P_{BAL}(t) \geq -Crate_{MAXd} * \Delta E_{ESS} \\ P_{ESS}(t) = P_{BAL}(t), P_{DEF}(t) = 0; \\ else \begin{cases} P_{ESS}(t) = -Crate_{MAXd} * \Delta E_{ESS} \\ P_{DEF}(t) = P_{BAL}(t) - P_{ESS}(t) \end{cases} \end{cases} \quad (4)$$

$$E_{ESS}(t) = E_{ESS}(t - \Delta t) + \eta_E * P_{ESS}(t - \Delta t) * \Delta t \quad (5)$$

$$E_{ESS}(t) = E_{ESS}(t - \Delta t) + P_{ESS}(t - \Delta t) * \Delta t \quad (6)$$

When $P_{DEF}(t)$ is empty at all the time steps of the considered time horizon, a configuration solution is established. This condition ensures the autonomy. We might have to do some iterations to achieve the right value of ΔE_{ESS} because of the power limitations and the ESS efficiency introduced in the validation block. In this case, we iterate the process and we calculate a new ΔE thanks to a new $P_{BAL}(t)$ profile from the power $P_{EX}(t)$ and $P_{DEF}(t)$ as shown in equation (7).

$$P_{BAL}(t) = P_{EX}(t) + P_{DEF}(t) \quad (7)$$

Next, we sum the ΔE value found in the new iteration to the ΔE_{ESS} value calculated in the previous iteration. An arrow represents this loop, from the validation bloc to the $E_{BAL}(t)$ definition bloc, in figure 1.

The calculated configurations give us the size of the potential PV array and the storage ΔE_{ESS} we have to install in order to ensure self-sufficiency. We save each solution, indexed by i, corresponding to a couple k_{PVi} and ΔE_{ESSi}.

After validation, the different solutions are compared in the solution assessment block (figure 1), according to different criteria defined by the user. To find the optimal solution, we propose to use the Pareto multi-objective optimization method. Thus, as explained in [12] and [13], we can define the optimal compromise between multiple criteria as the point in the Pareto front which have the minimal Euclidian distance to the utopia configuration. The utopia configuration corresponds to the configuration impossible to achieve at the minimum value of the two (or more) criteria. The selected configuration among all the i validated configurations is then the optimal size for self-sufficient and off-grid applications or, in future works, the minimal configuration that we can use in algorithms dedicated to connected MG design. Indeed, it would also be possible to start with this configuration and add a more complex EMS that would allow reducing the ESS and RES sizes by purchasing power from the main grid.

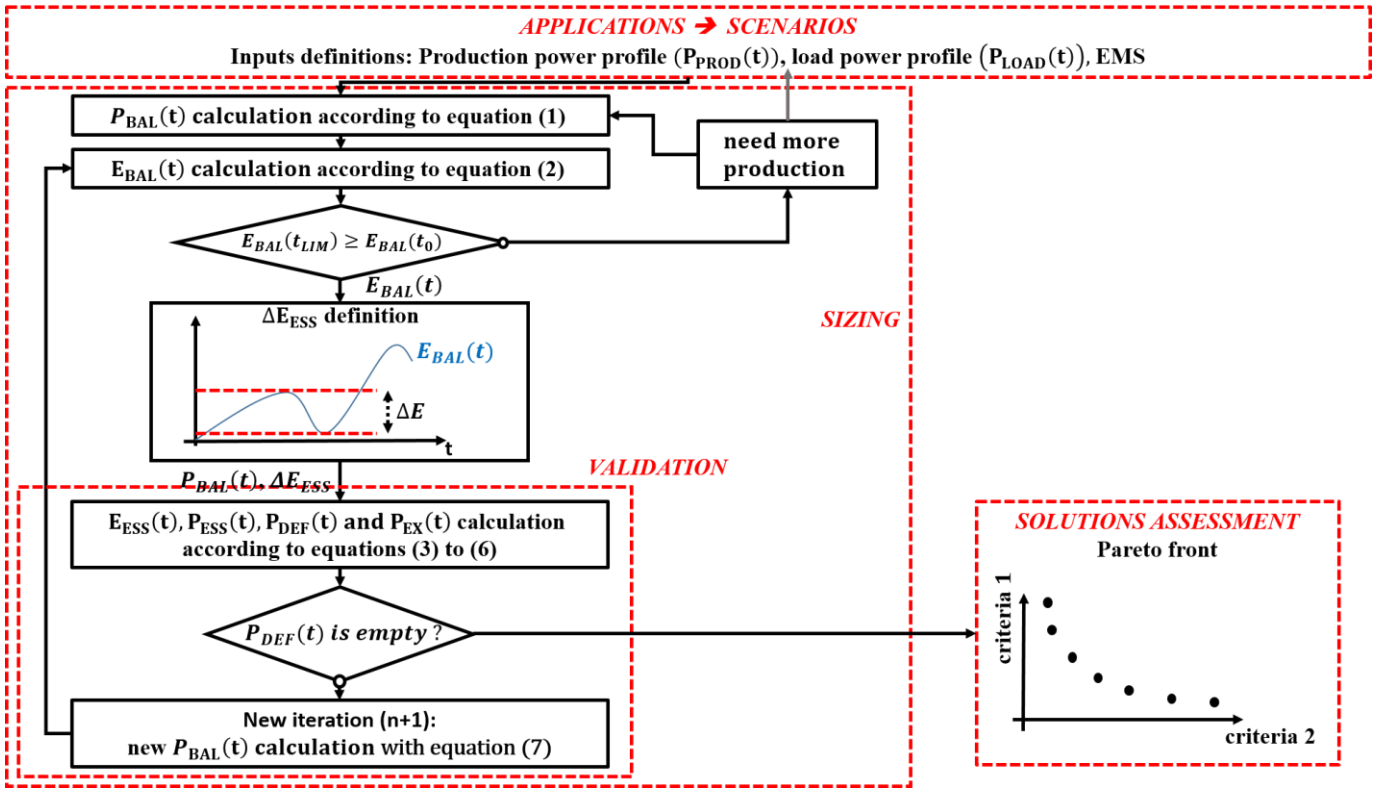

Figure 1. Flow chart diagram of the proposed sizing algorithm and methodology

At the end of the flowchart, we obtain the energy flow into the ESS, $E_{ESS}(t)$, and we can determine the state of charge (SoC) in terms of energy noted $SoE(t)$ with equation (8).

$$SoE(t) = \frac{E_{ESS}(t)}{\Delta E_{ESS}} \quad (8)$$

2.2 Power profiles inputs from the ADREAM BiPV database

The optimized energy BiPV in our laboratory, called ADREAM building is presented in figure 2.

Figure 2. ADREAM BiPV installations, experimental rooms and sensors and monitoring systems

It was built in 2012 at LAAS-CNRS, FRANCE. It has a 100 kWp of PV platform and more than 6500 sensors recording every minute [14]. Nowadays an experimental low voltage DC MG (LVDC MG) is deployed into the building to supply some servers and few low power DC equipment [15]. One of the project in this platform is to supply the DC loads of the entire ADREAM BiPV, such as electrical lighting network. In first approach, we apply our methodology in order to size the PV array and the ESS needed to supply the lighting network of the second floor of the building.

The inputs data of the sizing problem are:

- $P_{PV}(t)$: the power production of 1 kWp localized in the rooftop of the ADREAM building.
- $P_{LOAD}(t)$: the power consumed by the lighting network second floor.

Therefore, in our case, $P_{PROD}(t)$ use in equation (1) is calculate by equation (9) described below, where k_{PVi} is a scale factor that allows to change the PV source size between each configuration *i*.

$$P_{PROD}(t) = k_{PVi} * P_{PV}(t) \quad (9)$$

The power data selected to validate our approach correspond to two years (2016 and 2017) at one minute time step, Δt. This compromise between a relative small time step and the number of years allow us to consider intermittency due to cloudy days and seasonal changes while we keep a reasonable quantity of data.

The figure 3a shows the 2 years data set for an example of k_{PVi} equal 2.25 corresponding to 2.25 kWp of PV.

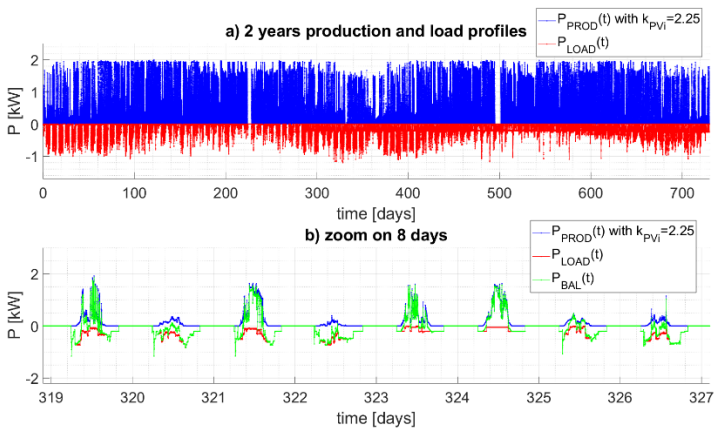

Figure 3. Consumption, production and balance power profiles of the ADREAM BiPV

We can see on the figure 3a the reduced PV production during the winter with an increase of the lighting network

consumption. The figure 3b shows a zoom on eight days and the $P_{BAL}(t)$ profile associated to $P_{PROD}(t)$ and $P_{LOAD}(t)$. We can see the production and consumption time shift during one day, with over production at the middle of the day and power deficit at the beginning and at the end of the day. We also see the high PV intermittencies during the day, due to clouds, relative high speed of wind or infrastructure shadows.

3. VRLAB BEHAVIOUR AND DEGRADATIONS

In order to qualify the operating conditions and to compare the different configurations according to the potential damages on ESS, we have to understand each degradation and why they occur. In this section, we present a review of the different degradations able to occur in VRLAB with short explanations of their consequences. We select such type of batteries because it is the technologies of ESS commonly used in MG stationary applications dedicated to buildings because of the low need of maintenance, low cost, high maturity implying a simple installation and its excellent rate of recyclability [16] [17] [18] [19] [20].

However, the main drawback of VRLAB technology is its short lifetime in case of RES operating conditions in particular with high and numerous intermittencies implying frequent incomplete cycles at partial state of charge (pSoC). It exits two approaches to improve the VRLAB lifetime. The first one consists in adding new materials or changing battery plate geometries and the other one consists in managing the power flow through the batteries. This paper contributes in the second approach. We focus on the damages due to operating conditions affecting the battery efficiency and the cyclic lifetime and we deduce five indicators. We do not consider the calendar lifetime [17], either the potential manufacturing damages.

3.1 Working principle of lead-acid battery

The main chemical processes occurring in lead acid batteries during their charge and discharge can be sum up as below:

- In discharge, crystals of lead sulfate are created respectively by lead dioxide reduction at the positive plate and lead oxidation on the negative plate [21]. This reaction, called sulphation, implies that crystals of lead sulfate gradually cover the electrodes surfaces and the battery capacity available progressively reduce until there is not enough active mass (AM). During the discharge, the electro-chemical reactions produce water, inducing a decrease of the acid concentration in the electrolyte.
- In charge, reversible electro-chemical reactions occur, thus the crystals of lead sulfate are reduced in lead at the negative plate and oxidized in lead dioxide at the positive plate [22]. During the charge, the reaction progressively consume water involving the increase of acid concentration in the electrolyte. Figure 4 represents the current and voltage evolutions during a battery charge at a constant current rate (C-rate) called CC phase. The voltage starts to grow exponentially when the water electrolysis becomes predominant [23]. At this stage, the battery produces a certain quantity of oxygen and hydrogen respectively at the positive and the negative plates by water decomposition. To ensure a complete charge limiting the water losses, the degassing effect and a thermal increase, it is recommended to follow the CC charge by a constant voltage (CV) phase (CC-CV charge protocol) [21] (figure 4). The battery is fully charged when the current value reaches to the floating current value. It is assumed that for a complete charge following a complete discharge, the CV phase starts at 80% of the battery capacity [24]. However other authors consider that this limit depends on the charge current and the SoC [25]. We can also notice that during CV phase, the battery efficiency changes and can be drastically reduced [24]. The main advantage of sealed VRLAB compared to classical vented/flooded lead acid batteries is the treatment of the water electrolysis by using the oxygen cycle and gasses recombination [26]. This technique reduces the rate of oxygen and hydrogen production and the water depletion, and reduces significantly the maintenance. However, this internal oxygen cycle is not a perfectly full reaction and the valve makes escape a small portion of hydrogen. This little loss of water is unavoidable in VRLAB. The gasses recombination process is also a high source of heat inducing an increase of the battery temperature and a potential thermal runaway [27].

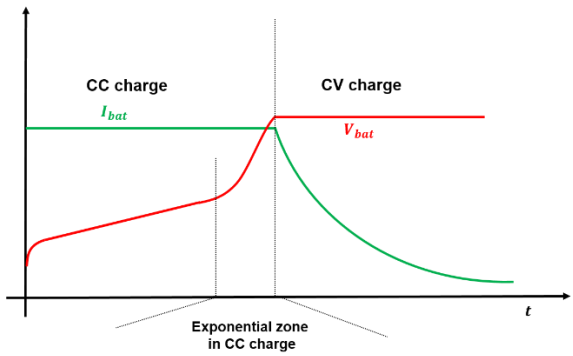

Figure 4. Typical voltage/current VRLAB characteristics during CC-CV charge

3.2 VRLAB stress factors and failure mechanisms

According to the principles presented above, we can bring out five main degradation processes affecting the VRLAB by increasing the internal resistance, involving capacity fade and potential short circuits. The following section presents each degradation mechanisms with their stress factors and the ways to minimize them. Figure 5 summarizes the main links.

- The corrosion affects the metallic part of the battery electrodes/plates, called grids or current collectors [28]. This damage appears mainly during overcharge, floating mode and CV charge [29] and it is due to the parasitic reaction. It is irreversible but it can be limited if the battery always works outside of these conditions.
- Hard or irreversible sulphation [30] is a significant worsening of the reversible sulphation reaction produced during discharge. If the crystals of lead sulfate are not destroyed with complete recharge, they gradually cover the AM surface and decrease the capacity of the battery by reducing the exchanging surface [10] [11]. They become more and more persistent if the complete recharge process is rarely achieved [31]. Thus, it is important to apply a regular complete charge to delete the entire lead surface.
- AM shedding, loosening or sludging correspond to an AM degradation, with loss of conductivity and loss of adherence to the grid [11]. It results of an excessive

changing in the AM morphology mainly caused by frequent incomplete cycle at partial SoC (pSoC), low C-rate at the beginning of the charging or battery overcharging [32].

- Electrolyte stratification is a non-homogeneous repartition of the electrolyte according to the vertical distribution inside the battery. This is due to the different density of the species, operating temperature and the natural gravity [33]. As explained previously, during the charge, the reaction consume water and the density of the electrolyte changes in a non-homogeneous way and gets denser near to the plates. The stratification process cannot be avoided but it is highly depending on the C-rate and can be enhanced by doing incomplete cycles, mainly at low pSoC [21] [33]. However it can be reversible if a complete charge with CV phase is done thanks to the water electrolysis and the degassing which helps to homogenize the electrolyte [34].
- Water losses are due to high external or internal temperatures and can cause damages to the battery and a potential thermal runaway [26]. An incomplete oxygen cycle with bad gasses recombination can be at the origin of an increase of internal temperature [27]. It can also be caused by electrolyte stratification and irreversible sulphation which blocks the gases flow [29].

The figure 5 synthesizes the VRLAB damages analysis with their causes and consequences. We can see that one cause can have multiple consequences. Moreover, as cited previously, all the consequences can affect others causes and all the damages are highly dependent and can increase other degradations. For this reason, it is very difficult to do a clear ~~a~~ hierarchy between damages. However, we propose to identify the main phenomena reducing prematurely the battery cyclic lifetime and how with some good practices we can reduce their causes. For example, we can notice that operating at pSoC with incomplete cycles increases the degradation of the AM, the sulphation and the stratification. Nevertheless, regular and complete CC-CV charges reduce these phenomena. Indeed doing a full charge with CV allows recovering some capacity and avoid hard sulphation and stratification. A patent made in 1998 [35] based on [36] applies this technique to improve the battery lifetime on hybrid pack of flooded lead acid batteries, charged with RES and dedicated to ancillary services into the main distribution grid. However, floating state and long periods at full charge increase the corrosion effect and water losses. The deep discharge and the use at high C-rate affect the battery capacity and increase the internal resistance.

We propose to consider a set of indicators or stress indexes calculate thanks to $P_{ESS}(t)$ and $SoE(t)$ able to quantify the uses that cause the cycle lifetime reduction:

- The number and repartition of incomplete cycles around pSoC with the level of the cycle amplitude,
- The time and the energy exchanged between two full charges,
- The time at full charge (considered SoE equal to 100%),
- The time at deep discharge,
- The C-rate in charging and discharging mode,

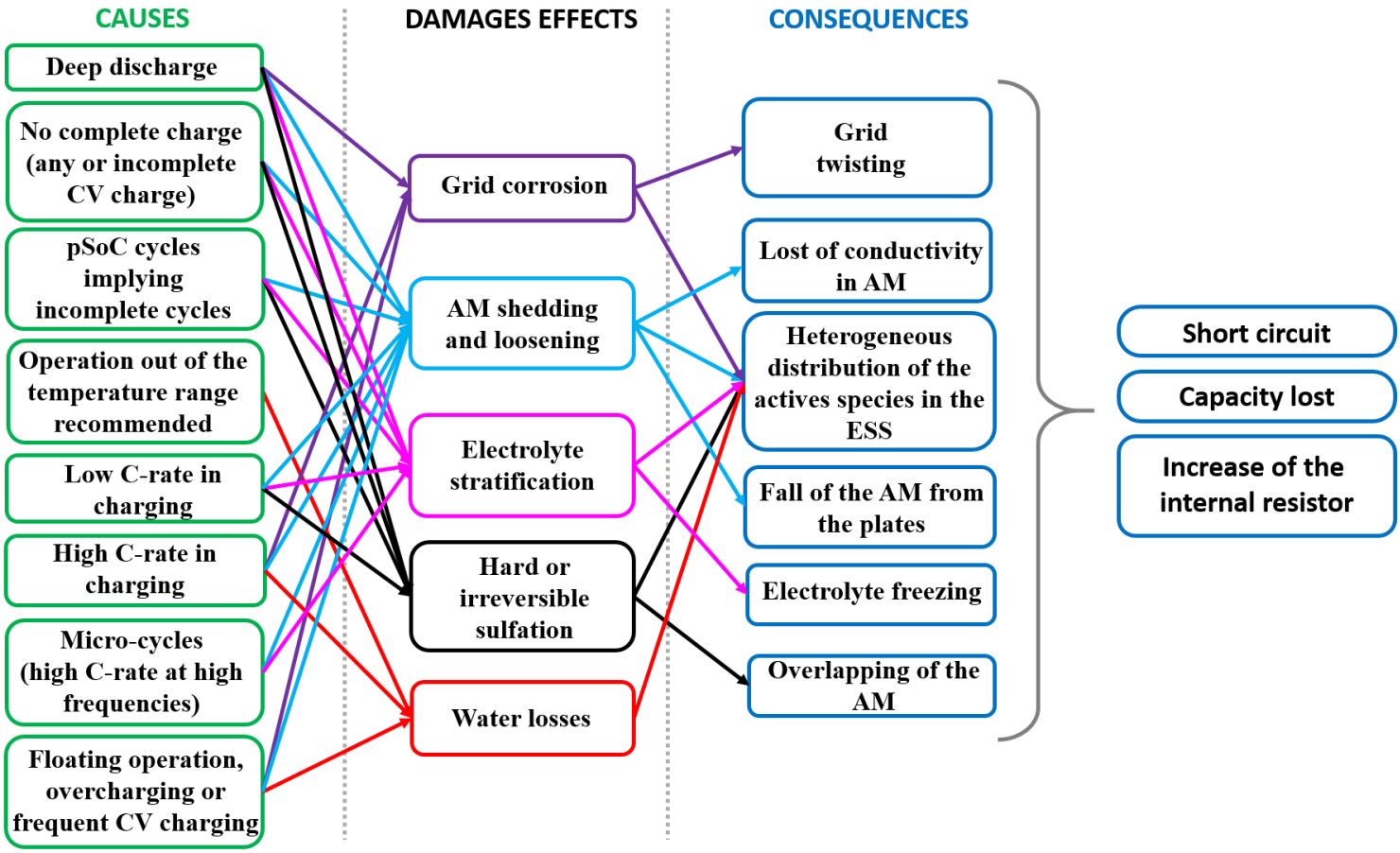

Figure 5. Potential damages with causes and consequences associated on VRLAB

4. RESULTS AND DISCUSSIONS

In this section, we compare four of the configurations obtained with the methodology presented in section 2 according to the five stress indexes present in section 3.

For the algorithm simulation, we set the time t_{LIM} on one year over the time horizon T equal to two years. We run the algorithm for the worst-case scenario by setting the initial value at t0 to the next local minimum value in the $E_{BAL}(t)$ profile. By doing this, we ensure to have the ESS at least one time empty all along the time horizon of the study. The variables used for the Pareto optimization are k_{PVi} and ΔE_{ESSi}. We choose to use directly these two variables, knowing that all criteria as cost or sustainability criteria depend on these variables. The k_{PVi} variable vary from 1 to 35 (corresponding to 1kWp to 35kWp), with a step equal to 0.25, which corresponds to a step of 250 Wp. Thus, we have 137 configurations, indexed by i, ensuring the lighting network self-sufficient operations. We limit the C-rate in charging and discharging respectively at 0.25C and 3C, and the ESS energy efficiency, η_E, is set at 0.85 according to [37] [18] and [38].

4.1 Pareto optimization sizing results

Thanks to the Pareto method, we optimize both the PV size according to k_{PVi} and the ESS size with ΔE_{ESSi}. As explained in section 2, the Pareto optimization allows to find the optimal configuration based on the minimum Euclidian distance to the utopia point. However, this optimal configuration can be different according to the normalization made on the parameters. In figure 6, we show the Pareto front and the optimal configuration obtained in case of two different types of normalization. The utopia point is spotted in red circle in figure 6. This figure shows two possible representations of the Pareto front. In figure 6a the Pareto curve is plot with the real values of k_{PVi} andΔE_{ESSi} and in figure 6b we plot the same set of configuration but when k_{PVi} and ΔE_{ESSi} are normalized, respectively between 0 to 1 and 0 to 3.

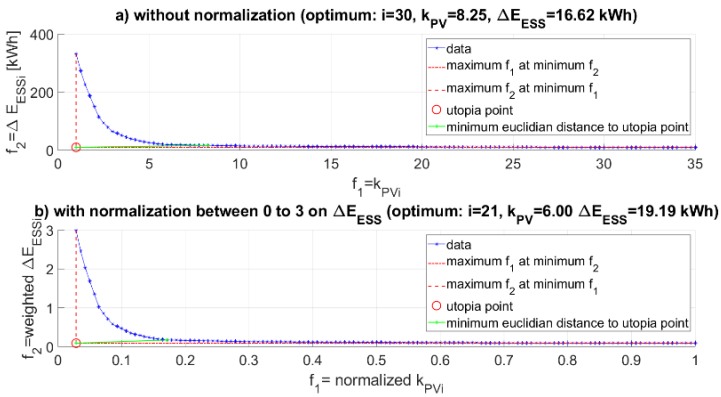

Figure 6. Pareto optimization and configurations results without and with normalization on k_{PVi} and ΔE_{ESSi}

Typically, it corresponds to a ratio of 3 between the kWp of PV and the kWh of ESS. We define this ratio as a weight between k_{PVi} and ΔE_{ESSi} and it is equal to the limit value of the ΔE_{ESSi} normalization. We choose it according to the ratio between the cost of a kWp of PV and a kWh of VRLAB. In our study, if we use directly the k_{PVi} and the ΔE_{ESSi} values, the optimal configuration is 8.25 kWp of PV plants and 16.62 kWh of batteries (for i 30). If we normalize the values of ΔE_{ESSi} and k_{PVi} we obtain another optimal configuration. The figure 7 shows the optimal configuration obtained with different normalizations on ΔE_{ESSi} and k_{PVi}. For each Pareto analysis, we normalize k_{PVi} from 0 to 1, and ΔE_{ESSi} from 0 to the ΔE_{ESS} weight.

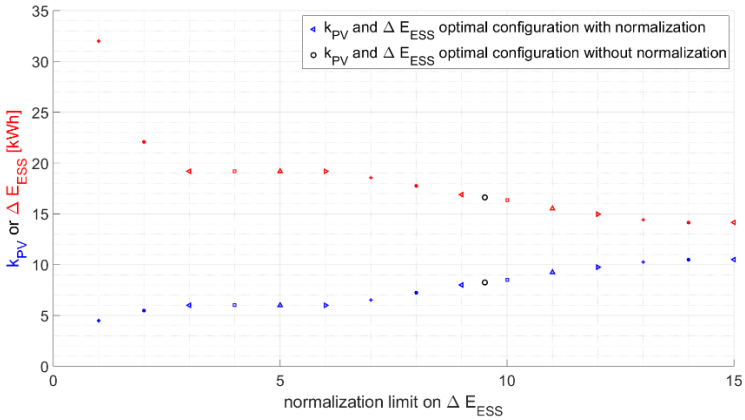

Figure 7. Sensibility of the optimal configuration results $(k_{PV}; \Delta E_{ESS})$ for different normalizations on ΔE_{ESS}

The optimal configuration found with Pareto method results to converge to 10kWp of PV panels and 14 kWh of ESS. The optimal configuration without weight and normalization (black circle on figure 7) corresponds to a ratio around 9.5 between the kWp of PV and the kWh of ESS. This study shows the impact of the weight factors on the optimization results. We can see that the quantity of PV needed for autonomy increases and ΔE_{ESSi} decreases when the weight factor on ΔE_{ESSi} increases. Indeed, when the weight on the storage system increase the optimal configuration correspond to an oversize PV source in order to minimize the size of ΔE_{ESSi}.

We validate our approach with four possible cases summarized in table 1.

Table 1. Configurations saved to comparative study

configuration number	i	k_{PVi} ∝[kWp]	ΔE_{ESSi} [kWh]	configuration description
1	1	1	332,87	minimum k_{PVi} and maximum ΔE_{ESSi} ensuring autonomy
2	30	8.25	16.62	optimal configuration ensuring autonomy, without normalization
3	21	6	19.19	optimal configuration ensuring autonomy with normalization between 0 to 3 for ΔE_{ESSi}
4	137	35	9.94	maximum k_{PVi} and minimum ΔE_{ESSi} ensuring autonomy

Figures 8 and 10 show the power exchanged with the ESS and the balance power profile (subplot b) for the two optimal configurations corresponding to the cases 2 and 3 with and without normalization. The figure 9 shows a zoom on 8 days of the power and SoE profiles for the configuration 2. On the figures 8 and 10, the cyan curve in the subplot (a) is the $SoE(t)$ profile. We see in figures 8b and 9 that during charging, the $P_{EES}(t)$ profile is more often limited at $Crate_{MAXc}$ than in configuration 3. Consequently, the $P_{EX}(t)$ values are greater,

even more during the summer periods. This is due to a higher size of the PV source in the configuration 2 because of a greater ratio between the PV kWp and the ESS kWh calculated without normalization and so equal to 9.5.

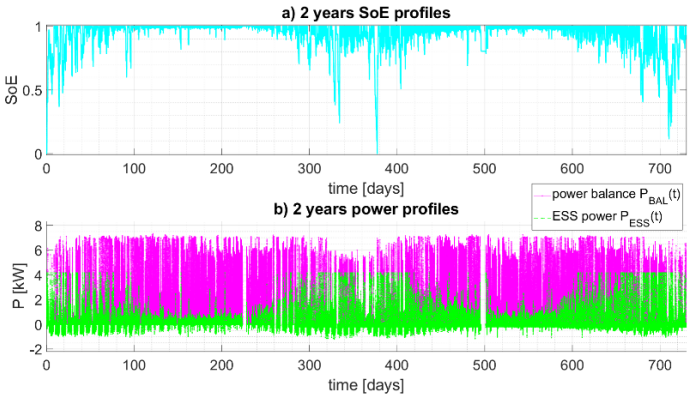

Figure 8. 2 years of power balance, ESS power and $SoE(t)$ profiles for the optimal configuration n° 2

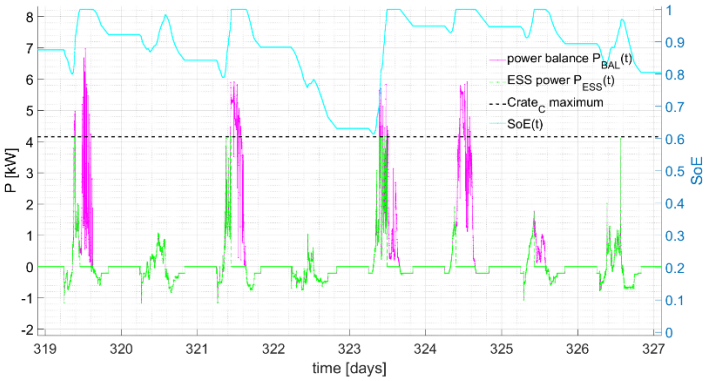

Figure 9. Zoom on 8 days of power balance, ESS power and $SoE(t)$ profiles for the optimal configuration n° 2

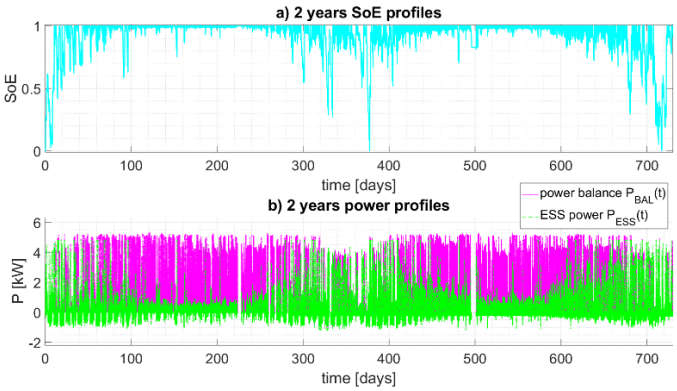

Figure 10. 2 years of power balance, ESS power and $SoE(t)$ profiles for the optimal configuration n° 3

In first approach, we fix the power limitations at a constant power rate in charging and discharging modes, $Crate_{MAXc}$ and $Crate_{MAXd}$, but this is true only if we consider the voltage of the ESS is constant. In reality, due to the voltage evolution during CC charging and discharging and the current decrease during CV charging, the power limits vary during these operating modes.

Thanks to the configurations presented in table 1 and the resulting ESS power and SoE profiles, we are able to identify and evaluate the stress factors implied by the working conditions on ESS, and more specifically on VRLAB.

4.2 Profiles analysis according to the VRLAB stress factors

4.2.1 C-rate impacts

The figure 11 shows the distribution of the C-rate in charging and discharging mode, respectively C $rate_c$ and $Crate_d$, during 2 years. In discharge (figure 11b) and for all the configurations, the C-rate is still inferior to the maximum C-rate limit, $Crate_{dMAX}$. Indeed, as we choose a strategy dedicated to improve autonomy, the ESS size have to satisfy the autonomy of the installation so its capacity is large enough to be far from the power limitations in discharging mode.

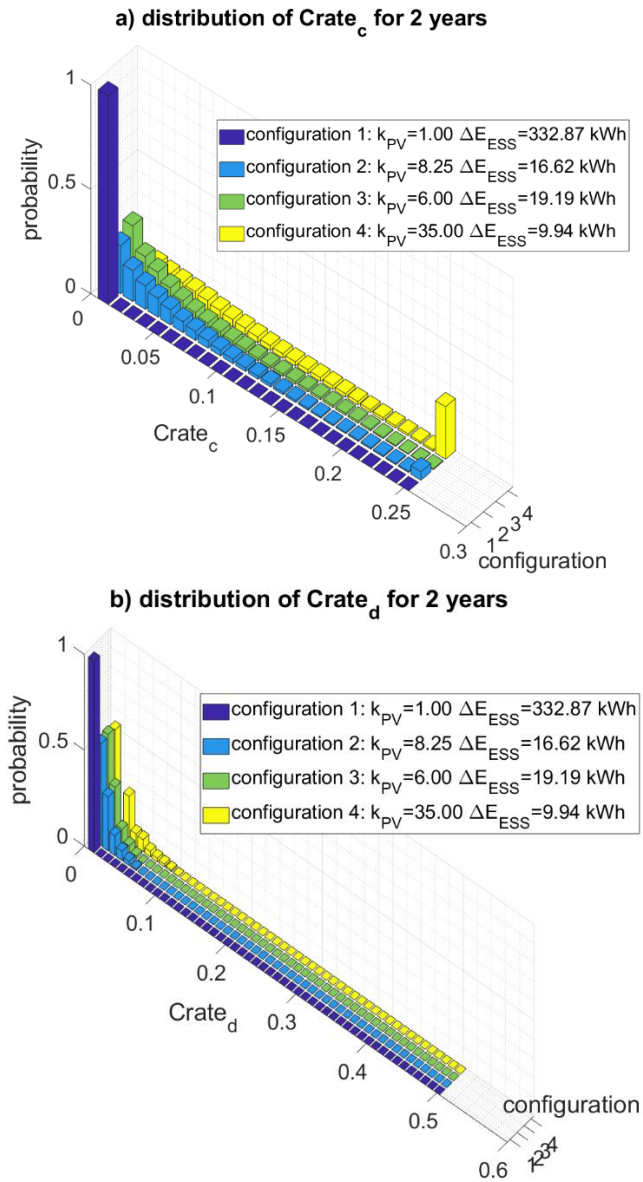

Figure 11. Distribution of the C-rate for the 4 different configurations in charging and discharging mode and for 2 years data set

The distribution of the C-rate in charge for the two optimal configurations is mainly at low C-rate, under 0.05C. It is an advantage to limit the VRLAB degradations because high C-rate damage the batteries, although it is specified that too low C-rate at the beginning of the charge can promote the AM shedding and hard sulphation. In case of configuration 1 and 4, the C-rate distribution in charge can become an issue

because the results mainly show very low C-rate in configuration 1 or very high C-rate in configuration 4.

4.2.2 SoC variations

In this subsection, we present the main results on the SoE fluctuations during 2 years. We are particularly interested by the time at full charge and at low SoE. We can see in figure 12 the ratio of time in the two years data set that the ESS stays at $SoE(t)$ equal to 100% (green points) or less than 30% (red points).

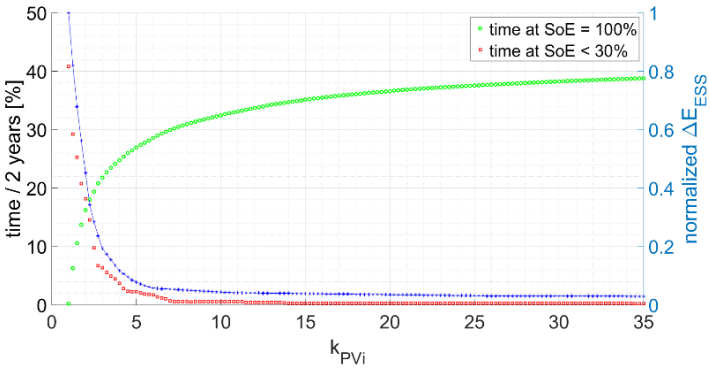

Figure 12. Cumulative time at $SoE(t)$ equal to 100% or less than 30% during two years, for all the configurations

The blue curve (right axis of the figure 12) reports the ESS size for all the validated configurations. We see in this figure that the duration when $SoE(t)$ is lower than 30% decreases with ΔE_{ESSi} and k_{PVi} increases. At the contrary, the consecutive time at $SoE(t)$ equal to 100% increases with k_{PVi} and ΔE_{ESSi} decreases. The first conclusion of this analysis is that the damages implied by low SoE (depth discharges) are not significant (lower than 5% for configuration with more than 5 kWp). This observation is confirmed by the $SoE(t)$ profile shown in figure 8 and 10. We observe that these low rates of discharge occur mainly during the winter. Concerning the charge, we see that the ESS is at SoE equal to 100% more than 25% of the time in case of configurations with k_{PVi} superior to 5 kWp and we see that full SoC mainly occur during summer. According to these observations and the mechanisms listed in section 3, it seems important to define clearly, what an $SoE(t)$ equal to 100% really means. Indeed, according to the model we used it is difficult to affirm that the battery is fully charged when $SoE(t)$ reaches 100% with a complete CC-CV charge. Moreover, we do not know how long the VRLAB stays at SoE equal to 100% between two discharges. If we assume that the full charge is reached when $SoE(t)$ is equal to 100%, it means that the battery operates often in floating operation mode during the two years, and this situation promotes corrosion and water losses. To avoid it, the VRLAB SoE could be limited at 80% but this implies to oversize the ESS and to not use the benefit of a complete charge, which mitigates the capacity loss due to sulphation and stratification.

Figure 13 represents the distribution of the time at $SoE(t)$ equal to 100% between 2 consecutive discharges, for the 4 configurations. For all the configurations, the maximum probability corresponds to a time at full SoE less than 0.1h. So, if the VRLAB is full when $SoE(t)$ reaches the value of 100%, the battery does not stay a long time in floating operation and consequently the impact of corrosion and water losses can be avoided. In the meantime, if the charge process is not fully achieved when the $SoE(t)$ reaches 100%, this duration does not ensure that the battery charge is complete before a new discharge.

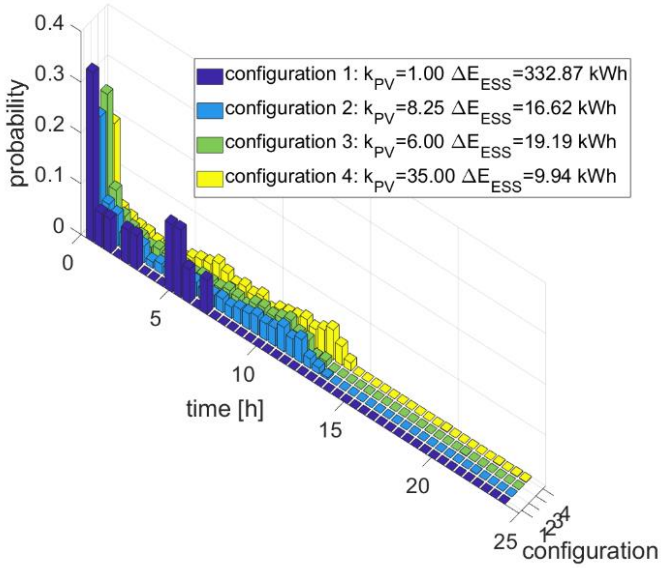

Figure 13. Distribution of the number of consecutive hours the ESS stays at SoE 100% for the 4 different configurations

The figure 14 shows the Watthours throughput discharged, according to the total ESS size, between two times at $SoE(t)$ equal to 100%. The Watthours throughput between two full charges appears to be less than 10% of the total ESS capacity in most of the cases. Thus, it is difficult to conclude on the impact on sulphation and stratification.

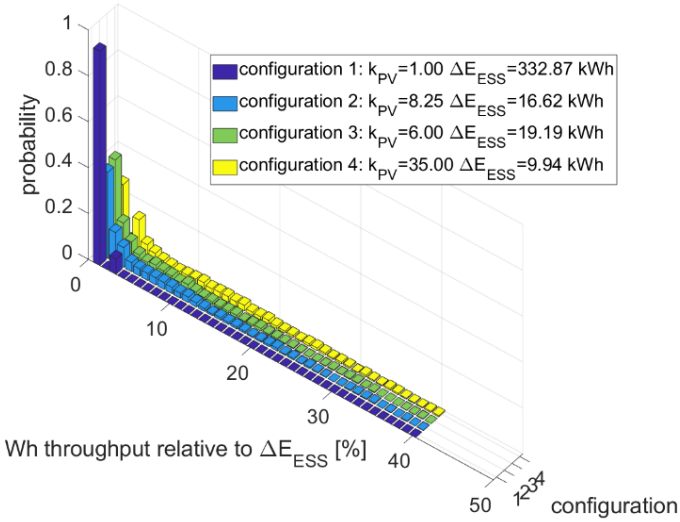

Figure 14. Distribution of the Watthours exchanged between two time at SoE 100% for the 4 different configurations

The figure 15 shows the distribution of the amplitude of each cycle around an average SoC in terms of energy, so noted pSoE.

We see that for the configuration 1 the cycle amplitudes are less than 10% in all the ranges of pSoE. Using the VRLAB in such conditions causes high risk of hard sulphation and stratification. Most of the incomplete cycles for the three other configurations (2, 3 and 4) occur above pSoE equal to 50%, which is coherent with the results presented in figure 12. The figure 15 allows concluding that working at incomplete cycle is typical of self-sufficient application. In our case, most of the

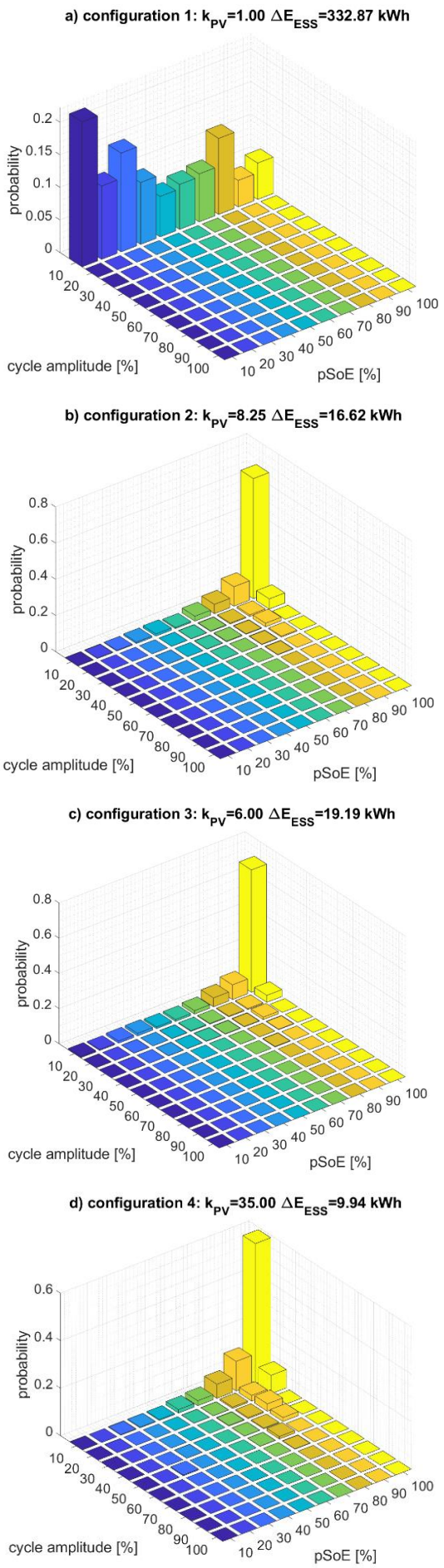

Figure 15. pSoE vs amplitude cycle histogram for each cycle of the $SOC_E(t)$ profile for 4 different configurations

pSoE are around 80% to 100% (more than 60% of the time between 90% and 100% of battery SoE).If we limit the SoE at 80%, the results will be a pSoE repartition mostly between 60%-80% range. Both operating conditions lead to degradations of the VRLAB, on one hand with corrosion and on the other hand with risking hard sulphation. Moreover, by using the VRLAB between 80% and 100% of SoE, we mostly solicit the battery when the efficiency is lower than in the CC charge phase. A solution would be to operate at SoE less than 80% but to ensure full CC-CV recharge on a regular basis in order to recover capacity because of the stratification and hard sulphation mechanisms. Nevertheless, this also highlights that we need a more accurate charge model in order to define the power limitations and the limit between CC and CV phases, according to the VRLAB SoE.

5. CONCLUSIONS AND PERSPECTIVES

This paper proposes an algorithm to size ESS and RES for self-sufficient operation in BiPV MG. This algorithm allows studying the typical power variations without taking into account a complex ESS model. We compare our results according to our stress indexes based on literature review, of the batteries ageing mechanisms. Four configurations are tested. We show that in the cases of optimal sizing, the ESS SoE mainly stays over 60%. However, in the range 60%-100% of SoE the batteries do many incompletes cycles (with amplitude cycle less than 20% of the ESS size). The C-rate during discharge and charge and the frequency of deep discharges do not have significant impacts on ESS.

According to these observations and the potential degradations of VRLAB listed in section 3, we can conclude that the stratification, the AM shedding and the sulphation mechanisms have a high influence on the VRLAB performances and in particular in the reduction of their capacities. In addition, the risk of premature corrosion and water losses resulting of frequent operations at high SoC have to be estimated. Moreover, as the VRLAB efficiency decreases in CV phase, as well as the potential power admitted by the battery, we recommend limiting the working operations during CV charging phase. Nevertheless, CV charging operations have positive impacts by avoiding hard sulphation and stratification, if the full charge is completely achieved.

To improve our actual approach, we propose to develop an accurate model of the maximum power during charge and the transition between CC and CV phases. Such a model will be very useful to manage the VRLAB charge in order to minimize the corrosion and avoid overcharges while we ensure the benefit of a complete charge. Moreover, this model will improve our sizing algorithm by considering power limitations and-different efficiencies during CC and CV phases. However, we have to keep in mind that the power limitations model should be simple in terms of parameters identification and execution.

A solution to manage the duration at full charge and optimize the VRLAB uses would be to split the ESS into several ESS. This ESS could mainly work at pSoE around 50% to avoid corrosion and water losses and sometimes fully recharged to avoid stratification. The strategy could switch between the different elements of the hybrid ESS to ensure CV phases. This search leads to find the optimal compromise between full charge benefits, as avoid hard sulphation and stratification and to limit corrosion and water losses phenomena in over charge.

Finally, the same approach could be possible with lithium-ion batteries or other types of ESS technologies and will be consider in the future.

REFERENCES

[1] M. Sechilariu, B. Wang, et F. Locment, « Building-integrated microgrid: Advanced local energy management for forthcoming smart power grid communication », *Energy Build.*, vol. 59, p. 236-243, avr. 2013, doi: 10.1016/j.enbuild.2012.12.039.

[2] D. Y. Yamashita, I. Vechiu, et J.-P. Gaubert, « A review of hierarchical control for building microgrids », *Renew. Sustain. Energy Rev.*, vol. 118, p. 109523, févr. 2020, doi: 10.1016/j.rser.2019.109523.

[3] A. J. Marszal *et al.*, « Zero Energy Building – A review of definitions and calculation methodologies », *Energy Build.*, vol. 43, nº 4, p. 971-979, avr. 2011, doi: 10.1016/j.enbuild.2010.12.022.

[4] F. Martin-Martínez, A. Sánchez-Miralles, et M. Rivier, « A literature review of Microgrids: A functional layer based classification », *Renew. Sustain. Energy Rev.*, vol. 62, p. 1133-1153, sept. 2016, doi: 10.1016/j.rser.2016.05.025.

[5] J. M. Lujano-Rojas, R. Dufo-López, J. L. Atencio-Guerra, E. M. G. Rodrigues, J. L. Bernal-Agustín, et J. P. S. Catalão, « Operating conditions of lead-acid batteries in the optimization of hybrid energy systems and microgrids », *Appl. Energy*, vol. 179, p. 590-600, oct. 2016, doi: 10.1016/j.apenergy.2016.07.018.

[6] M. Carpintero-Rentería, D. Santos-Martín, et J. M. Guerrero, « Microgrids Literature Review through a Layers Structure », *Energies*, vol. 12, nº 22, p. 4381, nov. 2019, doi: 10.3390/en12224381.

[7] M. F. Zia, M. Benbouzid, E. Elbouchikhi, S. M. Muyeen, K. Techato, et J. M. Guerrero, « Microgrid Transactive Energy: Review, Architectures, Distributed Ledger Technologies, and Market Analysis », *IEEE Access*, p. 1-1, 2020, doi: 10.1109/ACCESS.2020.2968402.

[8] M. Sufyan, N. A. Rahim, M. M. Aman, C. K. Tan, et S. R. S. Raihan, « Sizing and applications of battery energy storage technologies in smart grid system: A review », *J. Renew. Sustain. Energy*, vol. 11, nº 1, p. 014105, janv. 2019, doi: 10.1063/1.5063866.

[9] C. Gamarra et J. M. Guerrero, « Computational optimization techniques applied to microgrids planning: A review », *Renew. Sustain. Energy Rev.*, vol. 48, p. 413-424, août 2015, doi: 10.1016/j.rser.2015.04.025.

[10] A. Jossen, J. Garche, et D. U. Sauer, « Operation conditions of batteries in PV applications », *Sol. Energy*, vol. 76, nº 6, p. 759-769, 2004, doi: 10.1016/j.solener.2003.12.013.

[11] V. Svoboda *et al.*, « Operating conditions of batteries in off-grid renewable energy systems », *Sol. Energy*, vol. 81, nº 11, p. 1409-1425, nov. 2007, doi: 10.1016/j.solener.2006.12.009.

[12] M. Cheikh, B. Jarboui, T. Loukil, et P. Siarry, « A Method for Selecting Pareto Optimal Solutions in Multiobjective Optimization », p. 12.

[13] T. Terlouw, T. AlSkaif, C. Bauer, et W. van Sark, « Multi-objective optimization of energy arbitrage in community energy storage systems using different battery technologies », *Appl. Energy*, vol. 239, p. 356-372, avr. 2019, doi: 10.1016/j.apenergy.2019.01.227.

[14] LAAS-CNRS, « ADREAM project », *LAAS-CNRS - ADREAM project*. https://www.laas.fr/public/fr/le-projet-adream (consulté le janv. 10, 2017).

[15] J. Dulout, C. Alonso, L. Séguier, et B. Jammes, « Development of a photovoltaic low voltage DC micro-grid for buildings with energy storage systems », Toulouse,France, 2017, p. 7.

[16] B. Zakeri et S. Syri, « Electrical energy storage systems: A comparative life cycle cost analysis », *Renew. Sustain. Energy Rev.*, vol. 42, p. 569-596, févr. 2015, doi: 10.1016/j.rser.2014.10.011.

[17] O. Palizban et K. Kauhaniemi, « Energy storage systems in modern grids—Matrix of technologies and applications », *J. Energy Storage*, vol. 6, p. 248-259, mai 2016, doi: 10.1016/j.est.2016.02.001.

[18] A. B. Gallo, J. R. Simões-Moreira, H. K. M. Costa, M. M. Santos, et E. Moutinho dos Santos, « Energy storage in the energy transition context: A technology review », *Renew. Sustain. Energy Rev.*, vol. 65, p. 800-822, nov. 2016, doi: 10.1016/j.rser.2016.07.028.

[19] G. J. May, A. Davidson, et B. Monahov, « Lead batteries for utility energy storage: A review », *J. Energy Storage*, vol. 15, p. 145-157, févr. 2018, doi: 10.1016/j.est.2017.11.008.

[20] BCI, « Battery Council International ». https://batterycouncil.org/default.aspx (consulté le mars 05, 2019).

[21] D. Berndt, « Valve-regulated lead-acid batteries », *J. Power Sources*, p. 18, 2001.

[22] D. Linden, « Handbook of batteries », *Fuel Energy Abstr.*, vol. 4, nº 36, p. 265, 1995.

[23] A. M. Hardman, « A comparison of flooded, gelled and absorptive-separator lead/acid cells », *J. Power Sources*, vol. 23, nº 1-3, p. 127-134, mai 1988, doi: 10.1016/0378-7753(88)80058-2.

[24] J. Büngeler, E. Cattaneo, B. Riegel, et D. U. Sauer, « Advantages in energy efficiency of flooded lead-acid batteries when using partial state of charge operation », *J. Power Sources*, vol. 375, p. 53-58, janv. 2018, doi: 10.1016/j.jpowsour.2017.11.050.

[25] M. Cugnet et B. Y. Liaw, « Effect of discharge rate on charging a lead-acid battery simulated by mathematical model », *J. Power Sources*, vol. 196, nº 7, p. 3414-3419, avr. 2011, doi: 10.1016/j.jpowsour.2010.07.089.

[26] D. Valkovska, M. Dimitrov, T. Todorov, et D. Pavlov, « Thermal behavior of VRLA battery during closed oxygen cycle operation », *J. Power Sources*, vol. 191, nº 1, p. 119-126, juin 2009, doi: 10.1016/j.jpowsour.2008.10.014.

[27] G. Lodi, J. McDowall, et S. Rosellini, « VRLA battery aging characteristics », in *Proceedings of Intelec'96 - International Telecommunications Energy Conference*, Boston, MA, USA, 1996, p. 52-58, doi: 10.1109/INTLEC.1996.572378.

[28] D. J. Spiers et A. D. Rasinkoski, « Predicting the service lifetime of lead acid bat in photovoltaic systems », *J. Power Sources*, vol. 53, p. 245-253, 1995.

[29] P. Ruetschi, « Aging mechanisms and service life of lead–acid batteries », *J. Power Sources*, vol. 127, nº 1-2, p. 33-44, mars 2004, doi: 10.1016/j.jpowsour.2003.09.052.

[30] F. Mattera, D. Benchetrite, D. Desmettre, J. . Martin, et E. Potteau, « Irreversible sulphation in photovoltaic

batteries », *J. Power Sources*, vol. 116, nº 1-2, p. 248-256, juill. 2003, doi: 10.1016/S0378-7753(02)00698-5.
[31] E. Ebner, M. Gelbke, E. Zena, M. Wieger, et A. Börger, « Temperature-dependent formation of vertical concentration gradients in lead-acid-batteries under pSoC operation – Part 2: Sulfate analysis », *Electrochimica Acta*, vol. 262, p. 144-152, févr. 2018, doi: 10.1016/j.electacta.2017.12.046.
[32] E. Meissner, « How to understand the reversible capacity decay of the lead dioxide electrode », *J. Power Sources*, vol. 78, nº 78, p. 99-114, 1999, doi: 10.1016/S0140-6701(00)90784-7.
[33] E. Ebner, A. Börger, M. Gelbke, E. Zena, et M. Wieger, « Temperature-dependent formation of vertical concentration gradients in lead-acid batteries under PSoC operation – Part 1: Acid stratification », *Electrochimica Acta*, vol. 90, p. 219-225, févr. 2013, doi: 10.1016/j.electacta.2012.12.013.
[34] A. Jossen, « Fundamentals of battery dynamics », *J. Power Sources*, vol. 154, nº 2, p. 530-538, mars 2006, doi: 10.1016/j.jpowsour.2005.10.041.
[35] J. Alzieu, J.-C. Camps, et H. Smimite, « Procede de commande d'une centrale electrique associee a une source d'energie temporellement aleatoire », 98 08531, 1998.
[36] J. Alzieu, H. Smimite, et C. Glaize, « Improvement of intelligent battery controller: state-of-charge indicator and associated functions », *J. Power Sources*, vol. 67, nº 1-2, p. 157-161, juill. 1997, doi: 10.1016/S0378-7753(97)02508-1.
[37] S. Ould Amrouche, D. Rekioua, T. Rekioua, et S. Bacha, « Overview of energy storage in renewable energy systems », *Int. J. Hydrog. Energy*, vol. 41, nº 45, p. 20914-20927, déc. 2016, doi: 10.1016/j.ijhydene.2016.06.243.
[38] A. Poullikkas, « A comparative overview of large-scale battery systems for electricity storage », *Renew. Sustain. Energy Rev.*, vol. 27, p. 778-788, nov. 2013, doi: 10.1016/j.rser.2013.07.017.

NOMENCLATURE

Abbreviations

AM	Active Materials/Mass (in lead-acid battery)
BiPV	Building integrated PhotoVoltaic
CC	Constant Current
C-rate	Current rate
CV	Constant Voltage
DC	Direct Current
EMS	Energy Management System
ESS	Energy Storage System
LVDC	Low Voltage Direct Current
MG	Micro Grid
PMS	Power Management System
pSoC	partial State of Charge
RES	Renewable Energy Sources
SoC	State of Charge
VRLAB	Valve Regulated Lead Acid Battery

Variables

$Crate_c$	C-rate during ESS charging mode, C
$Crate_d$	C-rate during ESS discharging mode, C
$E_{BAL}(t)$	Energy balance, kWh
$E_{ESS}(t)$	Energy flow through the ESS, kWh
k_{PVi}	Coefficient to scale the PV plants installed in configuration i
$P_{BAL}(t)$	Power balance, kW
$P_{DEF}(t)$	Deficit power, kW
$P_{ESS}(t)$	ESS power, kW
$P_{EX}(t)$	PV power in excess, kW
$P_{LOAD}(t)$	Load power, kW
$P_{PROD}(t)$	Production power, kW
$SoC(t)$	ESS state of charge
$SoE(t)$	ESS state of energy
$DoD_E(t)$	ESS depth of discharge in terms of energy
ΔE	Energy decrease calculated on E(t) profile, kWh
ΔE_{ESSi}	Energy needed in storage for configuration i, kWh

Parameters

$Crate_{MAXc}$	ESS maximum current rate in charging mode
$Crate_{MAXd}$	ESS maximum current rate in discharging mode
t_{LIM}	Limit of time to verify the condition on energy profile, h
t_0	Initial time
T	Time horizon
Δt	Time step, h
η_E	ESS energy efficiency

Indices

t	Time
i	Configurations indices